

RSC Advances



This is an *Accepted Manuscript*, which has been through the Royal Society of Chemistry peer review process and has been accepted for publication.

Accepted Manuscripts are published online shortly after acceptance, before technical editing, formatting and proof reading. Using this free service, authors can make their results available to the community, in citable form, before we publish the edited article. This *Accepted Manuscript* will be replaced by the edited, formatted and paginated article as soon as this is available.

You can find more information about *Accepted Manuscripts* in the [Information for Authors](#).

Please note that technical editing may introduce minor changes to the text and/or graphics, which may alter content. The journal's standard [Terms & Conditions](#) and the [Ethical guidelines](#) still apply. In no event shall the Royal Society of Chemistry be held responsible for any errors or omissions in this *Accepted Manuscript* or any consequences arising from the use of any information it contains.

Rational design of a pyrene based luminescent porous supramolecular framework: excimer emission and energy transfer

Komal Prasad,^a Ritesh Haldar,^a and Tapas Kumar Maji^{ab*}

^a Molecular Materials Lab, New Chemistry Unit, Jawaharlal Nehru Centre for Advanced Scientific Research, Jakkur, Bangalore- 560064, India. ^b Chemistry and Physics of Materials Unit, Jawaharlal Nehru Centre for Advanced Scientific Research, Jakkur, Bangalore-560064, India.

*E-mail: tmaji@jncasr.ac.in. Tel: (+91) 80 2208 2810; Fax: (+91) 80 2208 2766

Abstract

Here we report rational design and synthesis approach to construct a porous luminescent supramolecular framework by modulating the spatial arrangement of aromatic linker directed by coordination to metal ion. A metal-organic complex, $\{\text{Cd}(\text{oxo-pba})_2(\text{H}_2\text{O})_2\}_n$ (**1**) has been synthesized using a functionalized pyrene linker, 1-pyrene- γ -oxo-butyric acid (oxo-pba) and this structure is extended to a 2D supramolecular framework through non-covalent interactions. Using Zn(II) as a metal center we have also synthesized $\{[\text{Zn}(\text{oxo-pba})_2(\text{bpy})]\cdot 4\text{H}_2\text{O}\}_n$ (**2**), which has similar chemical structure as compound **1**, except 2,2'-bipyridine chelator is occupied the positions of the coordinated water molecules. Further, compound **2** extends *via* several π - π and C-H $\cdots\pi$ interactions to form a 3D porous supramolecular structure as supported by CO₂ (195 K) and different solvents vapour adsorption studies. Compounds **1** and **2** both show bright pyrene excimer emission. Furthermore, the porosity and aromatic π electron decorated pore surface of compound **2** has been exploited for noncovalent encapsulation of a suitable acceptor dye acridine orange (AO) and an efficient energy transfer from the framework to encapsulated dye was observed.

Introduction

The macroscopic properties of a metal-organic solid depend on its molecular arrangement in the crystal lattice.¹ Therefore the ability to predict the spatial organization of the constituent metal ions and ligands in metal-organic compounds based on their structure and the metal ion geometry is invaluable for designing magnetic^{2a-2b} and optoelectronic materials^{2c-2d} and also for their nonlinear optical activity,^{2e} solid state reactivity^{2f} and zeolite-like porous properties.^{2g} Recently, there has been an increased interest in the design of various excimer or exciplex based optoelectronic materials for the development of sensors and light emitting diodes.³ Such materials based on inorganic-organic hybrid systems are relatively unexplored. Coordination driven spatial organization of various organic chromophores would be beneficial, as it enables efficient intermolecular charge transfer or energy transfer based on different donor-acceptor pairing in a close proximity and secondly it can restrict molecular rotation of the fluorophores that enhances their luminescence efficiencies.^{4a-4d} Therefore, the luminescence properties of such hybrid systems may be modulated with wavelength shifts, intensity changes or even new emission with the increase lifetimes as well as the quantum efficiencies.^{4e-4f} Among the different organic fluorophores pyrene and its derivatives have been extensively studied in the area of OLEDs due to its high luminescence quantum yield and life time.⁵ The large aromatic π surface area of pyrene can form strong $\pi\cdots\pi/C-H\cdots\pi$ association with other molecules resulting in a bright red shifted excimer or exciplex emission.⁶ Indeed luminescent metal-organic porous framework constructed using such chromophoric linker would be an exciting platform for molecular recognition based on guest responsive tunable emission, molecular sensing and light harvesting application and these are yet to be properly explored.⁷ In this communication, we have chosen a functionalized pyrene linker, 1-pyrene- γ -oxo-butyric acid (oxo-pba) and Cd(II) as a precursor to synthesize a molecular complex, $\{Cd(oxo-pba)_2(H_2O)_2\}_n$ (**1**). Similar to compound **1**, another molecular complex of Zn(II), $\{[Zn(oxo-pba)_2(bpy)]\cdot 4H_2O\}_n$ (**2**) has been synthesized, where *cis* coordinated water molecules of **1** is occupied with 2,2'-bipyridine (bpy). Such replacement changes 2D supramolecular nonporous network of **1** to a 3D porous supramolecular framework **2** with permanent porosity sustained by noncovalent $\pi\cdots\pi/C-H\cdots\pi$ interactions (Scheme 1). Both the compounds show pyrene based bright excimer emission and in framework

2 such emission has been further exploited for energy transfer application by encapsulating a suitable acceptor dye acridine orange (AO).

Experimental Section

Materials

All the reagents were commercially available and used as provided without further purification. Metal salts were obtained from SDFCL, 1-pyrene- γ -oxo-butyric acid (oxo-pba) and 2,2'-bipyridine (bpy) were obtained from Sigma Aldrich chemicals. Acridine orange hydrochloride hydrate was purchased from Acros Organics.

Synthesis of $\{\text{Cd}(\text{oxo-pba})_2(\text{H}_2\text{O})_2\}_n$ (1)

A 10 mL aqueous solution of oxo-pba (0.120 g, 0.4 mmol) was prepared using 0.1 M KOH solution in a glass vial. 10 mL methanolic solution of $\text{Cd}(\text{NO}_3)_2 \cdot 4\text{H}_2\text{O}$ (0.062 g, 0.2 mmol) was added to the ligand solution before it was sealed and kept in the oven at 80 °C. Good quality single crystals were obtained after 24 hours. Yield: 79%. Anal. calcd. for $\text{C}_{40}\text{H}_{30}\text{O}_8\text{Cd}$: C, 63.96; H, 3.99. Found C, 64.01; H, 4.23. FT-IR (KBr pellet, 4000–400 cm^{-1}): 3451 (b), 3071 (m), 3038 (s), 2968 (s), 2922 (w), 2900 (s), 1672 (s), 1605 (m), 1593 (s), 1565 (s), 1540 (w), 1508 (s), 1495 (s), 1473 (s), 1441 (s), 1406 (b), 1383 (s), 1372 (m), 1345 (s), 1313 (s), 1251 (s), 1232 (s), 1210 (s), 1192 (s), 1178 (s), 1158 (s), 1120 (s), 1078 (s), 1057 (s), 1025 (s), 992 (s), 972 (w), 959 (w), 954 (s), 880 (s), 845 (s), 820 (w), 802 (s), 776 (s), 736 (s), 720 (s), 694 (w), 682 (s), 652 (s).

Synthesis of $\{\text{Zn}(\text{oxo-pba})_2(\text{bpy}) \cdot 4\text{H}_2\text{O}\}_n$ (2)

A 10 mL aqueous solution of oxo-pba (0.120 g, 0.4 mmol) prepared using 0.1 M KOH and 10 mL methanolic bpy (0.031 g, 0.2 mmol) solution were mixed together and stirred for 30 minutes. $\text{Zn}(\text{NO}_3)_2 \cdot 6\text{H}_2\text{O}$ (0.059 g, 0.2 mmol) was dissolved in 10 mL water. 2 mL of this Zn(II) solution was slowly and carefully layered above the mixed ligand solution using 1 mL buffer (2:1 of water and methanol) solution. Good quality yellow coloured crystals were obtained after 15 days. The crystals were separated and washed with water/methanol (1:1) mixture and air dried. Yield: 81%. Anal. calcd. for $\text{C}_{50}\text{H}_{42}\text{N}_2\text{O}_{10}\text{Zn}$: C, 67.55; H, 4.73; N, 3.15. Found C, 68.13; H, 4.27; N, 3.03. FT-IR (KBr pellet, 4000–400 cm^{-1}): 3450 (b), 3071 (m), 3038 (s), 2968 (s), 2920 (w), 2900 (s), 1672 (s), 1605 (m), 1593 (s), 1565 (s), 1540 (w), 1508 (s), 1490 (s), 1473 (s), 1441 (s),

1406 (b), 1383 (s), 1345 (s), 1313 (s), 1251 (s), 1232 (s), 1210 (s), 1192 (s), 1178 (s), 1166 (w), 1158 (s), 1120 (s), 1078 (s), 1058 (s), 1025 (s), 1015 (w), 992 (s), 972 (w), 954 (s), 917 (m), 880 (s), 845 (s), 820 (w), 802 (s), 776 (s), 736 (s), 720 (s).

Bulk amount of the compound was synthesized in powder form by the direct mixing of the corresponding ligand solution with aqueous solution of Zn(II).

Synthesis of acridine orange (AO) included 2a (AO@2)

0.03 g of desolvated compound **2** was dipped in 10^{-1} mM methanol solution of acridine orange (AO) dye. The mixture was then stirred for 48 hours, filtered, washed with fresh methanol and dried to obtain AO@2. NMR spectroscopy of AO@2 suggest that 0.08 molecule of AO encapsulated of **2** per formula. Anal. cald. for $C_{51.36}H_{35.52}N_{2.24}O_6Zn$: C, 75.22; H, 4.34; N, 3.83. Found C, 75.97; H, 4.11; N, 3.61. FT-IR (KBr pellet, $4000-400\text{ cm}^{-1}$): 3450 (b), 3071 (m), 3038 (s), 2968 (s), 2920 (w), 2900 (s), 2851 (w), 1672 (s), 1604 (w), 1594 (s), 1566 (m), 1540 (w), 1506 (s), 1489 (s), 1472 (s), 1441 (s), 1419 (s), 1384 (s), 1373 (m), 1346 (s), 1253 (s), 1232 (s), 1210 (s), 1191 (w), 1180 (s), 1157 (s), 1141 (m), 1123 (s), 1076 (s), 1058 (s), 1042 (w), 1026 (s), 1015 (w), 995 (s), 978 (w), 956 (s), 885 (s), 846 (s), 820 (w), 801 (s), 777 (s), 737 (s), 718 (s), 696 (m), 683 (s), 654 (s), 633 (s).

Physical measurements

Elemental analyses were carried out using a Thermo Fischer Flash 2000 Elemental Analyzer. FT-IR spectra were recorded on a Bruker IFS 66v/S spectrophotometer using KBr pellets in the region $4000-400\text{ cm}^{-1}$. Thermogravimetric analysis (TGA) was carried out (Metler Toledo) in nitrogen atmosphere (flow rate = 50 mL min^{-1}) in the temperature range $30-600^\circ\text{C}$ (heating rate = 5°C min^{-1}). Powder X-ray diffraction (PXRD) pattern of the products were recorded on a Bruker D8 Discover instrument using Cu-K α radiation. Electronic absorption spectra were recorded on a Perkin Elmer Lambda 900 UV-vis Spectrometer and PL spectra were taken with Perkin-Elmer model LS 55 luminescence spectrometer. NMR spectrum was obtained with a Bruker AVANCE 400 (400 MHz) Fourier transform NMR spectrometer with chemical shifts reported in parts per million (ppm). Fluorescence lifetime measurements were carried out using the EPL-405 ps pulsed diode laser. The quantum yields (QY) were determined using 'integrating sphere', an absolute QY measurement system.

X-ray crystallography

X-ray single crystal structural data of **1** and **2** were collected on a Bruker Smart-CCD diffractometer equipped with a normal focus, 2.4 kW sealed tube X-ray source with graphite monochromated Mo-K α radiation ($\lambda = 0.71073 \text{ \AA}$) operating at 50 kV and 30 mA. The program SAINT⁸ was used for integration of diffraction profiles and absorption correction was made with SADABS⁹ program. All the structures were solved by SIR 92¹⁰ and refined by the full matrix least-squares method using SHELXL-97.¹¹ All the hydrogen atoms were fixed by HFIX and placed in ideal positions. Potential solvent accessible area or void space was calculated using the PLATON multipurpose crystallographic software.¹² All crystallographic and structure refinement data of **1** and **2** are summarized in Table 1. Selected bond lengths and angles for **1** and **2** are given in Tables S2-S5. All calculations were carried out using SHELXL 97, PLATON, SHELXS 97¹³ and WinGX system, Ver 1.70.01.¹⁴ The cif files are deposited in Cambridge crystallographic database with CCDC number 987769-987770.

Adsorption study

Adsorption isotherms of N₂ (77 and 195 K) and CO₂ (195 K) were recorded using the desolvated sample of **2** by using a QUANTACHROME QUADRASORB-SI analyzer. In the sample tube, the adsorbent sample (~100–150 mg) was placed which had been prepared at 80 °C under a 1×10^{-1} Pa vacuum for about 12 h prior to measurement of the isotherms. Helium gas (99.999% purity) at a certain pressure was introduced in the gas chamber and allowed to diffuse into the sample chamber by opening the valve. The amount of gas adsorbed was calculated from the pressure difference ($P_{\text{cal}} - P_{\text{e}}$), where P_{cal} is the calculated pressure with no gas adsorption and P_{e} is the observed equilibrium pressure. All the operations were computer controlled and automatic.

The adsorption isotherm of different solvents (MeOH, at 293 K and water, at 298 K) of **2** was measured in the vapour state by using a BELSORP-aqua volumetric adsorption instrument from BEL, Japan. A sample of about ~100–150 mg was prepared by heating at 150 °C for about 12 h under a vacuum (1×10^{-1} Pa) prior to measurement of the isotherms. The solvent molecules used to generate the vapour were degassed fully by repeated evacuation. Dead volume was measured with helium gas. The adsorbate was placed into the sample tube, then the change of the

pressure was monitored, and the degree of adsorption was determined by the decrease in pressure at the equilibrium state. All operations were computer controlled and automatic.

Results and discussion

Structural description of $\{\text{Cd}(\text{oxo-pba})_2(\text{H}_2\text{O})_2\}_n$ (**1**)

Compound **1**, synthesized in a solvothermal reaction of $\text{Cd}(\text{NO}_3)_2 \cdot 4\text{H}_2\text{O}$ and oxo-pba crystallizes in monoclinic $C2/c$ space group. The asymmetric unit consists of 0.5 Cd(II), one oxo-pba ligand and a water molecule (Fig. 1a). Each Cd(II) center is attached to four carboxylate oxygen atoms (O1, O2, O1_a and O2_a) from two oxo-pba and other two coordination sites are occupied by water molecules (O4 and O4_a) ($a = 2-x, y, 1/2-z$) (Table 1, S1 and S2). The two oxo-pba act as two side arms of **1**, and extend as 1D column along a -axis through slightly off-set face-to-face $\pi \cdots \pi$ interaction ($\text{cg} \cdots \text{cg}$ distance $\sim 3.496 \text{ \AA}$) between the pyrene rings (Fig. 1b and S1†). The dihedral angle between two pyrene rings is 77.2° and this is reinforced by H-bonding between coordinated waters (O5 and O6) and carboxylate oxygens (O8 and O1), respectively (Fig. S2 and S3†). This 1D column is extended to 2D along b -axis by another H-bonding between coordinated water molecule (O6) and carboxylate oxygen (O7) (2.657 \AA) (Fig. 1c-1d). Additional face-to-edge ($\sim 3.375 \text{ \AA}$) interactions between pyrene rings of neighbouring 1D chains also support such molecular packing (Fig. 1c-1d).

Structural description of $\{[\text{Zn}(\text{oxo-pba})_2(\text{bpy})] \cdot 4\text{H}_2\text{O}\}_n$ (**2**)

Further, we envisage the replacement of two *cis*-oriented coordinated water molecules (O5 and O6) in compound **1** by a chelating ligand bpy which has similar coordination angle for further modification in the structure. However, this was unsuccessful as suitable single crystal was not formed. But in a similar attempt with Zn(II) we could able to synthesize $\{[\text{Zn}(\text{oxo-pba})_2(\text{bpy})] \cdot 4\text{H}_2\text{O}\}_n$ (**2**). **2** crystallizes in monoclinic $C2/c$ space group and similar to compound **1** each hexa-coordinated Zn(II) attached to four oxygen atoms (O1, O1_a, O2 and O2_a) from two oxo-pba but two water molecules are replaced by two nitrogen atoms (N1, N1_a) from a chelating bpy (Fig. 2a and see Table 1 and S3-S4†). The overall molecular structure resembles **1**, however the dihedral angle between two pyrene rings in **2** significantly reduces to 60.4° due to steric strain imposed by bpy coordination (Fig. S2 and S4†). Two such mirror image complexes

pack in such a way that two bpy stacks in a face-to-face fashion (cg...cg distance = 4.230 Å) and two oxo-pba arms of each complex stack in a face-to-edge fashion (cg...cg distance = 3.601 Å) (Fig. 2b-2e). Such molecular packing leads to a 1D supramolecular column along *c*-direction that has four arms directing in *ab* plane (Fig. 2b). Further 1D columns with four arms are interdigitated by off-set face-to-face π - π stacking (cg...cg distance = 3.827 Å) between oxo-pba to form a 3D supramolecular framework with 1D distorted rectangular shaped channels ($6.2 \times 6.2 \text{ \AA}^2$) along *c*-direction (Fig. 2c).¹⁵ These channels are filled with hydrogen bonded guest water molecule (O1W) (Fig. 3 and S5†) and removal of all the water molecules create a void space of 15.7 % of total cell volume.¹⁶ Interestingly, the pore surface is decorated with the oxygen atoms from the carboxylate groups and also aromatic pyrene rings which render hydrophilic and phobic sites on the pore surface, respectively.

Thermal stability and flexibility

The phase purity of compound **1** is confirmed by the measurement of PXRD patterns of the as-synthesized compound (Fig. S6†). To verify the thermal stability of **2** TG analysis was carried out and it shows release of guest water molecules in the temperature range of 50-130 °C and the desolvated phase (**2a**) is stable upto 220 °C (Fig. S7†). This high thermal stability indicates very strong intermolecular association in **2**. The desolvated framework was prepared at 80 °C under reduced pressure (10^{-1} Pa) and PXRD pattern of the same shows subtle changes compared to that of as-synthesized pattern (Fig. S8†) suggesting structural transformation. Such sort of rearrangement or flexibility is expected in supramolecular structure and similar phenomena are well-known in literature.¹⁷ To get an insight of the structural change we have indexed the PXRD pattern of **2a** and observed a distinct change in the cell parameters compared to that of as-synthesized **2**. The cell parameters are as follows: $a = 15.018(14) \text{ \AA}$; $b = 13.149(16) \text{ \AA}$; $c = 9.790(28) \text{ \AA}$; $\beta = 98.23(8)^\circ$; $V = 1913.53 \text{ \AA}^3$ (ESI†). This result shows significant change along *a*-axis and cell volume also decreases to less than half compared to **2**. This suggests structural contraction after guest removal.

Gas and solvent vapour adsorption

To measure the porosity of **2a** we have carried out N₂ adsorption at 77 K and recorded a type-II adsorption profile (Fig. S9†). Interestingly, the CO₂ adsorption profile at 195 K shows stepwise and gradual uptake with increasing pressure and finally ended with a value ~ 28 mL/g at P = 1 atm (Fig. 4) indicating the permanent porosity in the framework. This sort of CO₂ adsorption is characteristics of ‘soft’ porous framework and this can be attributed to weak supramolecular forces that built up the overall framework of **2**.¹⁸ Further we have also carried out water (298 K) and methanol (293K) vapour adsorption to understand the polarity of the pores surface and structural flexibility (Fig. 5a). Water vapour uptake increases slowly at low pressure but at $P/P_0 \sim 0.7$ shows a distinct step to reach the final uptake amount ~ 100 mL/g that corresponds to ~ 3.7 molecules/formula. Desorption profile takes a different route leading to a large hysteresis. In case of methanol vapour initial uptake is very low, afterwards two distinct steps appear at $P/P_0 \sim 0.24$ and ~ 0.68 and final uptake amount corresponds to 2.6 molecules/formula (Fig. 5a). Methanol vapour shows slow uptake at low pressure and with increasing vapour pressure probably the structure expands to accommodate methanol molecules through specific interactions with hydrophobic and hydrophilic sites. Both vapour sorption profiles are suggesting the contracted pore in the desolvated state and presence of hydrophobic and-philic sites on the pore surface (Inset Fig. 5b). The stepwise uptake reiterates flexible nature of the supramolecular framework.

Photophysical properties: excimer emission and energy transfer

Both **1** and **2** contain pyrene as a chromophore and hence an intense emission characteristic was anticipated. **1** shows a broad absorbance spectrum with a maximum ~ 400 nm (Fig. S10†). Upon excitation at 330 nm, **1** shows a red shifted emission with a maximum at 500 nm (Fig. S10†). Such a huge red shift compared to oxo-pba monomer emission indicates formation of a pyrene excimer and this is also clear from the crystal structure of **1** where two pyrene moieties from two neighbouring complexes are in close proximity through $\pi \cdots \pi$ interaction (Fig. S11†). Similar to **1**, emission spectrum of **2** also shows a broad featureless band with a maximum at 490 nm ($\lambda_{\text{ex}} = 330$ nm) (Fig. S10†). Thus this cyan emission can be attributed to the intermolecular pyrene excimer formation. From crystal structure it is evident that the

pyrene rings, aligned in close proximity, are in appropriate spatial disposition to make such excimer. Time-resolved single-photon counting experiment of **2** upon excitation at 405 nm and monitoring at 490 nm showed a long lived excited state ($\sim \tau_1 = 0.4$ ns (4 %), $\tau_2 = 11.1$ ns (96 %)), further corroborating to excimer emission (Fig. 6b). oxo-pba dissolved in methanol (10^{-6} M) was found to have shorter life time ($\sim \tau_1 = 1.6$ ns) in the monomeric state compared to the life time of compound **2** (Fig. S12[†]).

The permanent porosity, amphiphilic nature of the pore surface and bright cyan excimer emission of compound **2** incited us to explore the energy transfer property by non-covalent encapsulation of a suitable acceptor dye molecule. We selected acridine orange (AO) dye as its absorbance maximum ($\lambda_{\text{max}} = 490$ nm) overlaps with the emission spectrum of **2** and the molecular dimensions is 13×6 Å² along the molecular axis of AO. The presence of four –CH₃ groups and large aromatic core of AO would help facile inclusion in the hydrophobic pore of **2**. The mixing of activated compound **2** in MeOH with 2 mol% of AO resulted the compound **AO@2**. The difference in PXRD patterns of **AO@2** with dehydrated **2** suggests structural reorganization after encapsulation of AO (Fig. S13[†]). To confirm that the AO dye has been encapsulated into the supramolecular pores of **2a**, we have measured the CO₂ adsorption isotherm of **AO@2** at 195 K. It shows only 18 mL/g of CO₂ uptake, which is much lesser than that in case of **2a** (Fig. 4). ¹H-NMR study of **AO@2** after disintegrating in DCl and elemental analysis suggest that 0.08 molecules of AO has been included per formula of **2** (Fig. S14[†]). Further, a physical mixture of compound **2** and AO was prepared in a 1:0.1 molar ratio. This physical mixture showed a similar final uptake amount as that of **2a** for CO₂ adsorption measurement at 195 K (Fig. S15[†]). The experiment proves that the pores of compound **2a** are not blocked by AO in case of physical mixture. A distinct absorption band around 500 nm for **AO@2** further concludes the inclusion of AO (Fig. S16[†]). When AO loaded compound **AO@2** is selectively excited at 330 nm, the excimer emission at 490 nm is significantly reduced and strong emission related to AO with maxima at 550 nm appeared (Fig. 6a, Fig. 6b Inset and Fig. S17[†]). This suggests an efficient Förster resonance energy transfer (FRET) from framework to non-covalently encapsulated dye molecules.^{7d,7h} Furthermore the excitation spectrum of **AO@2** monitored at AO emission (575 nm) shows a maximum at 410 nm which is clearly showing the contribution of **2** in the observed emission (Fig. S18[†]). Energy transfer is also realized from

direct excitation of **AO@2** at 500 nm that shows lesser intensity compared to when excited at 330 nm (Fig. S19†).

To further elucidate the energy transfer process we have carried out time-resolved single-photon counting experiments of **AO@2** with 405 nm excitation and monitored the emission at 470 (λ_{max} of donor) and 600 nm (for acceptor) (Fig. 6b and Fig. S20†). The life-time decreased significantly when monitored at 470 nm (~ 2.5 ns) compared to **2** (~ 11.5 ns) and at 600 nm we observed sufficiently high life-time (~ 4.1 ns) compared to only AO dye (3.2 ns). This shows that the framework emission energy has been consumed by the acceptor dye leading to decrease of life-time when observed at 470 nm. The absolute quantum yield of **2** and **AO@2** were also studied and found to be 6.1 and 17.5%, respectively. Such enhanced quantum yield in **AO@2** indicates importance of such dye encapsulated luminescent framework in terms of better luminescence efficacy.

Conclusions

In conclusion, a rational design approach has been implemented to construct a novel 3D supramolecular luminescent porous structure based on a molecular complex $\{\text{Zn}(\text{oxo-pba})_2(\text{bpy})\}$ as a building unit. We have shown how a small change in the metal coordination sphere acts as a structure directing force to generate an unprecedented soft porous framework structure. This framework shows bright cyan pyrene excimer emission and permanent porosity in the framework allows energy transfer application based on non-covalent encapsulation of an acceptor dye through FRET process. This sort of design of supramolecular soft framework would pave a new dimension towards luminescent material design for potential light harvesting applications.

Associated content

† Electronic Supplementary Information (ESI)

Acknowledgements

K. P and R. H acknowledge DST, Govt. Of India and JNCASR, Bangalore, India.

We also thank Dr. Ranjani Viswanatha and Avijit Saha for fluorescence lifetime and quantum yield measurements.

References

- 1 a) G. R. Desiraju, *J. Am. Chem. Soc.*, 2013, **135**, 9952; b) G. R. Desiraju, *Angew. Chem. Int. Ed.*, 2007, **46**, 8342; c) J. F. Stoddart, *Angew. Chem. Int. Ed.*, 2012, **51**, 12902; d) G. R. Desiraju, J. J. Vittal and A. Ramanan, *Crystal Engineering*, World Scientific, Singapore, 2011.
- 2 a) N. F. Sciortino, K. R. Scherl-Gruenwald, G. Chastanet, G. J. Halder, K. W. Chapman, J.-F. Létard and C. J. Kepert, *Angew. Chem. Int. Ed.*, 2012, **51**, 10154; b) A. Chakroborty, B. K. Ghosh, J. R. Arino, J. Ribas and T. K. Maji, *Inorg. Chem.*, 2012, **51**, 6440; c) R. Haldar, K. V. Rao, S. J. George and T. K. Maji, *Chem. Eur. J.*, 2012, **18**, 5848; d) M. D. Allendorf, C. A. Bauer, R. K. Bhakta and R. J. T. Houk, *Chem. Soc. Rev.*, 2009, **38**, 1330; e) L. Wen, L. Zhou, B. Zhang, X. Meng, H. Qu and D. Li, *J. Mater. Chem.*, 2012, **22**, 22603; f) L. R. MacGillivray, G. S. Papaefstathiou, T. Friššić, T. D. Hamilton, D.-K. Bučar, Q. Chu, D. B. Varshney and I. G. Georgiev, *Acc. Chem. Res.*, 2008, **41**, 280; g) K. S. Park, Z. Ni, A. P. Côté, J. Y. Choi, R. D. Huang, F. J. Uribe-Romo, H. K. Chae, M. O'Keeffe and O. M. Yaghi, *Proc. Natl. Acad. Sci. U.S.A.*, 2006, **103**, 10186.
- 3 a) N. Chandrasekharan and L. A. Kelly, *J. Am. Chem. Soc.*, 2001, **123**, 9898; b) B. P. Bag and P. K. Bharadwaj, *Org. Lett.* 2005, **7**, 1573; c) H. S. Jung, M. Park, D. Y. Han, E. Kim, C. Lee, S. Ham and J. S. Kim, *Org. Lett.* 2009, **11**, 3378; d) S. Nishizawa, Y. Kato and N. Teramae, *J. Am. Chem. Soc.*, 1999, **121**, 9463; e) J. Kalinowski, M. Cocchi, D. Virgili, V. Fattori, J. A. G. Williams, *Adv. Mater.*, 2007, **19**, 4000.
- 4 a) N. B. Shustova, B. D. McCarthy and M. Dincă, *J. Am. Chem. Soc.*, 2011, **133**, 20126; b) C. Y. Sun, X. L. Wang, X. Zhang, C. Qin, P. Li, Z. -M. Su, D. X. Zhu, G. G. Shan, K.

- J. Shao, H. Wu and J. Li, *Nat. Commun.*, 2013, **4**, 168; c) V. M. Suresh, A. De and T. K. Maji, *Chem. Commun.*, 2015, DOI: 10.1039/C5CC05453B; d) N. Sikdar, K. Jayaramulu, V. Kiran, K. V. Rao, S. Sampath, S. J. George and T. K. Maji, *Chem. Eur. J.*, 2015, **21**, 11701; e) V. M. Martínez, S. Furukawa, Y. Takashima, I. L. Arbeloa and S. Kitagawa, *J. Phys. Chem. C.*, 2012, **116**, 26084; f) B. D. McCarthy, E. R. Hontz, S. R. Yost, T. V. Voorhis and M. Dincă, *J. Phys. Chem. Lett.*, 2013, **4**, 453.
- 5 T. M. Figueira-Duarte and K. Müllen, *Chem. Rev.*, 2011, **111**, 7260.
- 6 a) B. D. Wagner, G. J. McManus, B. Moulton and M. J. Zaworotko, *Chem. Commun.*, 2002, 2176; b) G. J. McManus, J. J. Perry 4th, M. Perry, B. D. Wagner and M. J. Zaworotko, *J. Am. Chem. Soc.*, 2007, **129**, 9094; c) F. M. Winnik, *Chem. Rev.* 1993, **93**, 587; d) M. E. Gallina, B. Baytekin, C. Schalley and P. Ceroni, *Chem. Eur. J.*, 2012, **18**, 1528.
- 7 a) L. Sun, H. Xing, Z. Liang and J. Yu, R. Xu, *Chem. Commun.*, 2013, **49**, 11155; b) B. Chen, S. Xiang and G. Qian, *Acc. Chem. Res.*, 2010, **43**, 1115; c) C. A. Kent, B. P. Mehl, L. Ma, J. M. Papanikolas, T. J. Meyer and W. Lin, *J. Am. Chem. Soc.*, 2010, **132**, 12767; d) V. M. Suresh, S. J. George and T. K. Maji, *Adv. Funct. Mater.*, 2013, **23**, 5585; e) K. Jayaramulu, P. Kanoo, S. J. George and T. K. Maji, *Chem. Commun.*, 2010, **46**, 7906; f) Y. Cui, H. Xu, Y. Yue, Z. Gou, J. Yu, Z. Chen, J. Gao, Y. Yang, G. Qian and B. Chen, *J. Am. Chem. Soc.*, 2012, **134**, 3979; g) Y. Cui, Y. Yue, G. Qian and B. Chen, *Chem. Rev.*, 2012, **112**, 1126; h) R. Haldar, R. Matsuda, S. Kitagawa, S. J. George and T. K. Maji, *Angew. Chem. Int. Ed.*, 2014, **53**, 11772.
- 8 SMART (V 5.628), SAINT (V 6.45a), XPREP, SHELXTL; Bruker AXS Inc. Madison, Wisconsin, USA, 2004.
- 9 G. M. Sheldrick, Siemens Area Detector Absorption Correction Program, University of Göttingen, Göttingen, Germany, 1994.
- 10 A. Altomare, G. Cascarano, C. Giacovazzo and A. Gualaradi, *J. Appl. Cryst.*, 1993, **26**, 343.
- 11 G. M. Sheldrick, SHELXL-97, Program for Crystal Structure Solution and Refinement; University of Göttingen, Göttingen, Germany, 1997.
- 12 A. L. Spek, *J. Appl. Crystallogr.*, 2003, **36**, 7.

- 13 G. M. Sheldrick, SHELXS 97, Program for the Solution of Crystal Structure, University of Göttingen, Germany, 1997.
- 14 L. J. Farrugia, WinGX-A Windows Program for Crystal Structure Analysis, *J. Appl. Cryst.*, 1999, **32**, 837.
- 15 The sizes of the channels were calculated considering the van der Waals radii of the atoms.
- 16 A. L. Spek, *J. Appl. Crystallogr.*, 2003, **36**, 7.
- 17 a) M. Kishan, J. Tian, P. K. Thallapally, C. A. Fernandez, S. J. Dalgarno, J. E. Warren, B. P. McGraila and J. L. Atwood, *Chem. Commun.*, 2010, **46**, 538; b) S. Bureekaew, H. Sato, R. Matsuda, Y. Kubota, R. Hirose, J. Kim, K. Kato, M. Takata and S. Kitagawa, *Angew. Chem. Int. Ed.*, 2010, **49**, 7660.
- 18 a) R. Haldar, S. K. Reddy, V. M. Suresh, S. Mohapatra S. Balasubramanian and T. K. Maji, *Chem. Eur. J.*, 2014, **20**, 4347; b) N. Yanai, K. Kitayama, Y. Hijikata, H. Sato, R. Matsuda, Y. Kubota, M. Takata, M. Mizuno, T. Uemura and S. Kitagawa, *Nat. Mater.*, 2011, **10**, 787; c) J. Seo, R. Matsuda, H. Sakamoto, C. Bonneau and S. Kitagawa, *J. Am. Chem. Soc.*, 2009, **131**, 12792; d) R. Haldar, K. L. Gurunatha, N. Sikdar and T. K. Maji, *Inorg. Chem. Front.*, 2015, **2**, 278.



Scheme 1 Schematic showing rational design of a luminescent porous supramolecular framework for light harvesting application.

Table 1 Crystal data and structure refinement parameters of **1** and **2**.

Parameters	Compound 1	Compound 2
Empirical formula	C ₄₀ H ₃₀ O ₈ Cd	C ₅₀ H ₄₂ N ₂ O ₁₀ Zn
Formula weight	751.05	888.18
Crystal system	Monoclinic	Monoclinic
Space group	C2/c	C2/c
<i>a</i> , Å	53.310(5)	30.904(5)
<i>b</i> , Å	5.4433(5)	16.245(5)
<i>c</i> , Å	11.0524(9)	8.387(5)
β , °	97.600(6)	90.170(5)
<i>V</i> , Å ³	3179.0(5)	4211(3)
<i>Z</i>	4	4
<i>T</i> , K	293	293
μ , mm ⁻¹	0.745	0.648
<i>D</i> _{calcd} , g/cm ³	1.569	1.401
<i>F</i> (000)	1528	1832
Reflections [<i>I</i> > 2σ(<i>I</i>)]	2791	2529
Unique reflections	3811	5111
Total reflections	15293	24178
<i>R</i> _{int}	0.097	0.090
GOF on <i>F</i> ²	1.02	0.85
<i>R</i> ₁ [<i>I</i> > 2σ(<i>I</i>)] ^a	0.0661	0.0571
<i>R</i> _w [all data] ^b	0.2170	0.1680

$$^a R_1 = \frac{\sum ||F_o| - |F_c||}{\sum |F_o|}; ^b R_w = \left[\frac{\sum \{w(F_o^2 - F_c^2)^2\}}{\sum \{w(F_o^2)^2\}} \right]^{1/2}$$

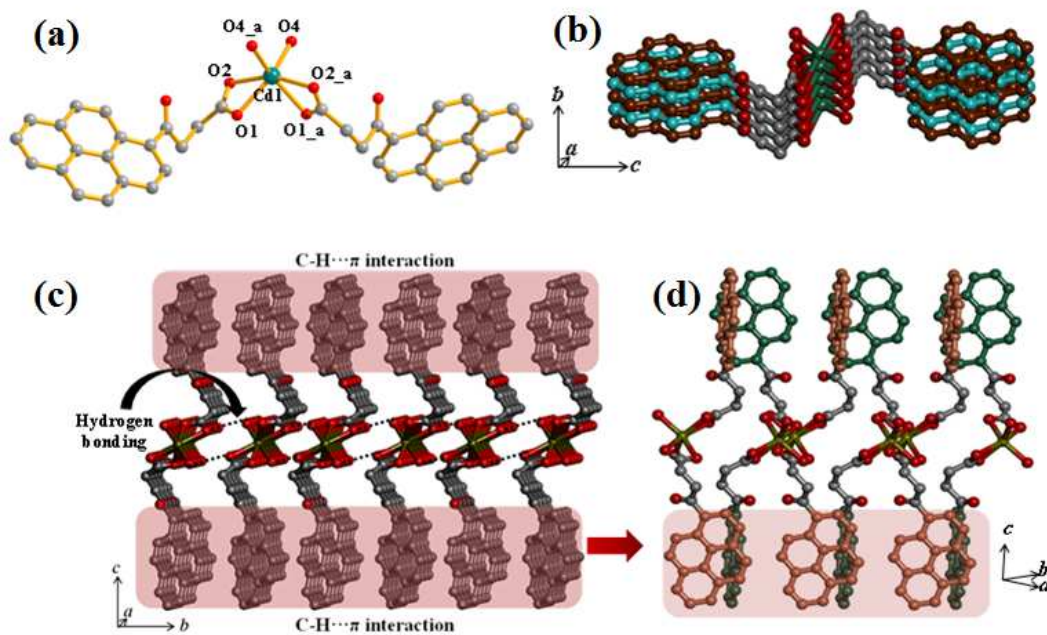


Fig. 1 (a) Coordination environment of Cd(II) in complex **1**; (b) 1D column like structure along *a*-axis; (c) View of the 2D structure formed via C-H \cdots π interaction between oxo-pba of neighbouring 1D columns in **1** and hydrogen bonding (black dotted lines) between O4 H \cdots O2 **1**; (d) View of the C-H \cdots π interactions between neighbouring oxo-pba (shown in two different colours for clarity).

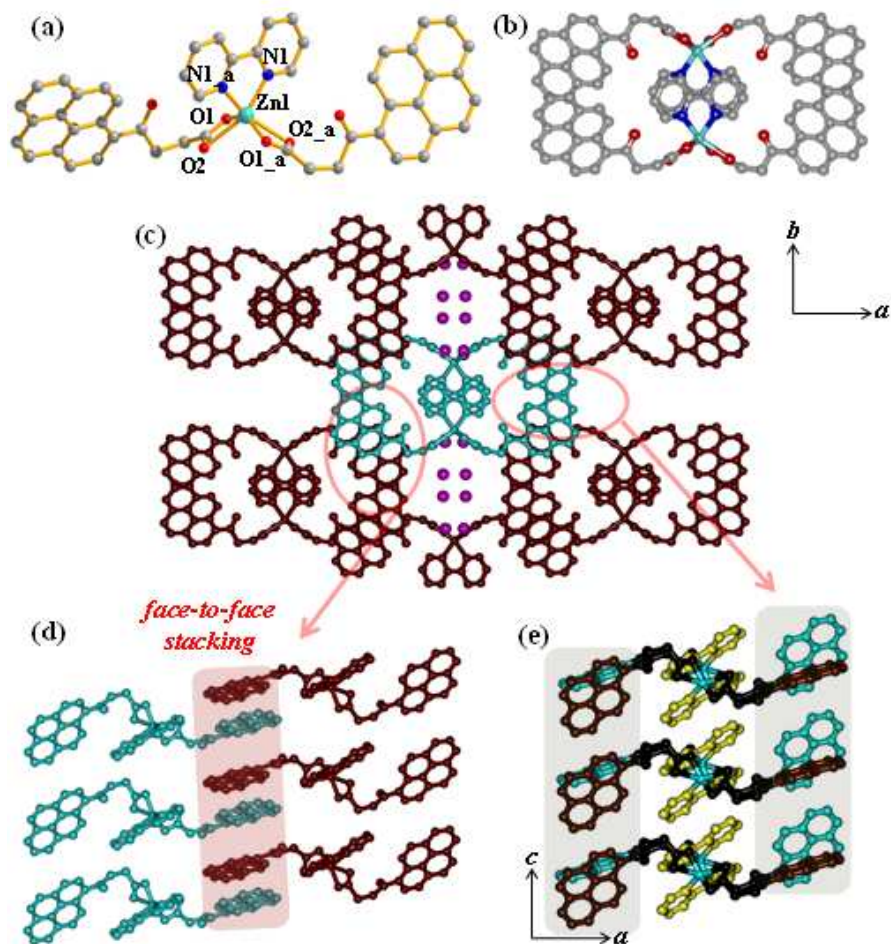


Fig. 2 (a) Coordination environment of Zn(II) in complex 2; (b) 1D supramolecular column with four arms; (c) 3D supramolecular structure of 2 with 1D pore filled with water molecules (pink balls); (d) two 1D columns interdigitated by face-to-face stacking of pyrene chromophores; (e) face-to-edge interaction between pyrene moieties.

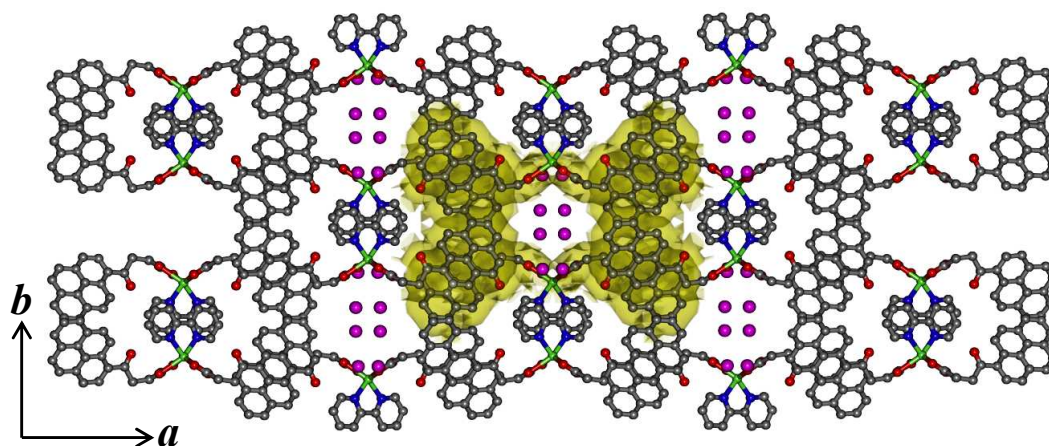


Fig. 3 View of 3D supramolecular framework of **2** built by several non-covalent interactions showing 1D water filled channels along the crystallographic *c*-axis.

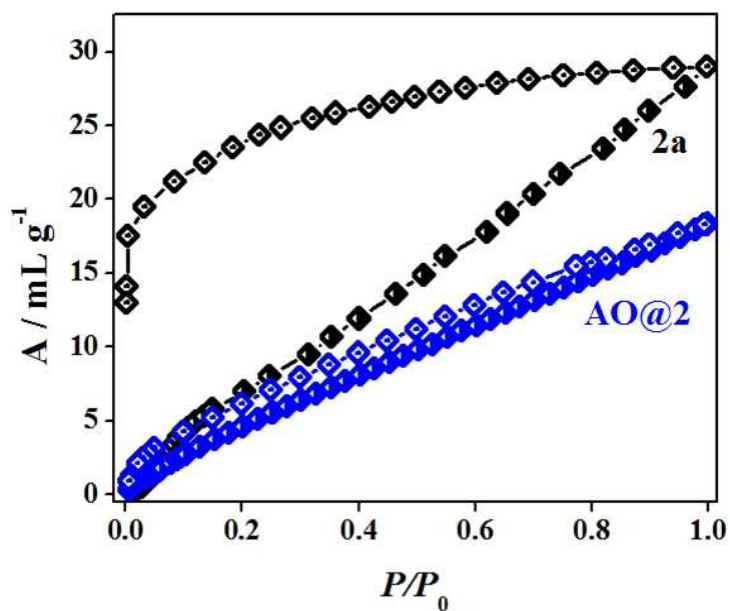


Fig. 4 CO₂ adsorption isotherm of **2a** and **AO@2** at 195 K.

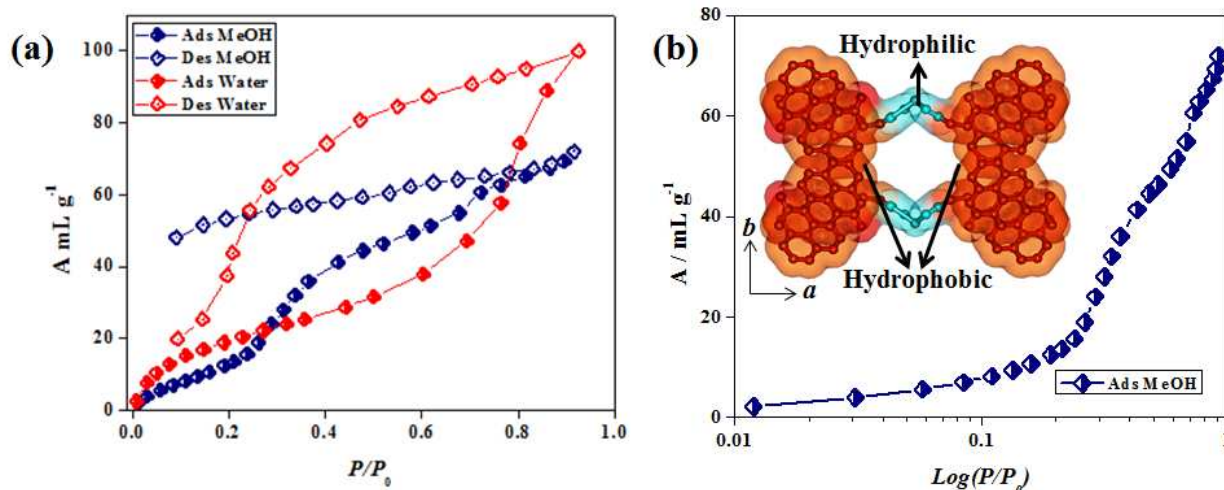


Fig. 5 (a) H₂O and MeOH vapour adsorption profiles of **2** at 298 and 293 K, respectively; (b) MeOH vapour adsorption profiles of **2** at 293 K in logarithmic scale; Inset shows hydrophobic and philic parts of the pore in **2**.

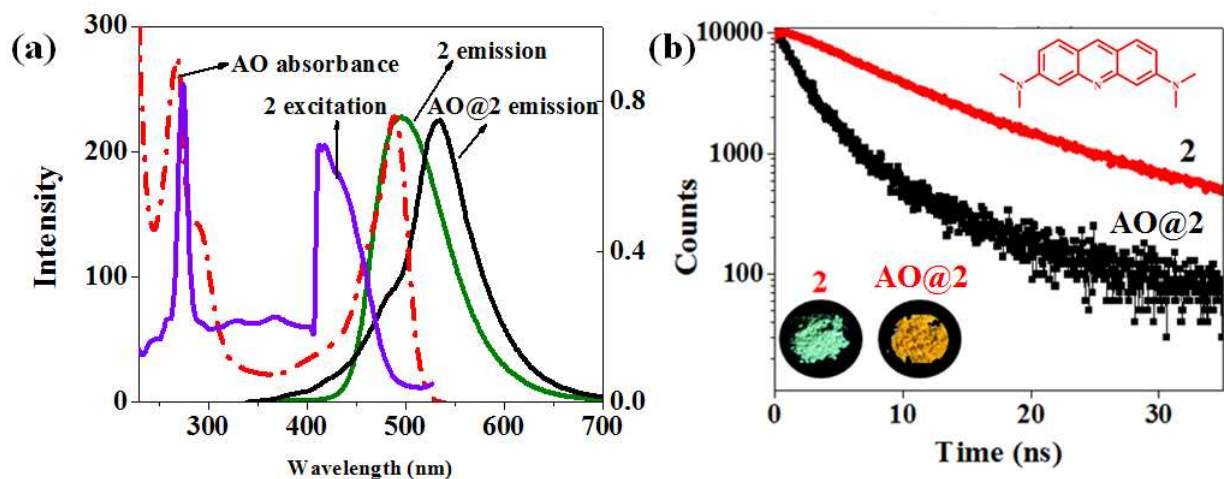


Fig. 6 (a) Emission spectra of **2** and **AO@2** upon excitation at 330 nm; excitation spectrum of **2** monitored at 540 nm; UV-vis absorption spectrum of AO in methanol; (b) Fluorescence life time profiles of **2** and **AO@2** monitored at 470 nm upon excitation at 405 nm; Inset: Structure of Acridine orange (AO).